Quantitative Prediction of Long-Term Failure of Polycarbonate

E. T. J. Klompen, T. A. P. Engels, L. C. A. van Breemen, P. J. G. Schreurs, L. E. Govaert,* and H. E. H. Meijer

Dutch Polymer Institute (DPI), Section Materials Technology (MaTe), Eindhoven, University of Technology, P.O. Box 513, NL-5600 MB, Eindhoven, The Netherlands

Received March 8, 2005; Revised Manuscript Received May 26, 2005

ABSTRACT: Time-to-failure of polymers, and the actual failure mode, are influenced by stress, temperature, processing history, and molecular weight. We show that long-term ductile failure under constant load is governed by the same process as short term ductile failure at constant rate of deformation. Failure proves to originate from the polymer's intrinsic deformation behavior, more particularly the true strain softening after yield, which inherently leads to the initiation of localized deformation zones. In a previous study, we developed a constitutive model that includes physical aging and is capable of numerically predicting plastic instabilities. Using this model the ductile failure of polycarbonates with different thermal histories, subjected to constant loads, is accurately predicted also for different loading geometries. Even the endurance limit, observed for quenched materials, is predicted and it is shown that it originates from the structural evolution due to physical aging that occurs during loading. For low molecular weight materials this same process causes a ductile-to-brittle transition. A quantitative prediction thereof is, however, outside the scope of this paper and requires a more detailed study.

1. Introduction

The viscoelastic nature of polymers has a big influence on their deformation and failure behavior, since their response to different excitations strongly depends on the time scale of the experiment. An implication is that a polymer loaded well below its tensile strength, as determined in a short-term test, may not sustain this load indefinitely. Classical examples are failure of polymers subjected to long-term static (creep) and dynamic (fatigue) loading.[1,2]

The failure of polymers subjected to a long-term static load, generally referred to as creep rupture, is often accompanied by a significant amount of plastic deformation, including the formation of a neck.[3,4] Sometimes the actual failure, either ductile or brittle, is preceded by prerupture processes like stress-whitening, cracking, or crazing[3−6] and, although these can play an important role in the final failure behavior, particularly in active environments,[7] they are not dealt with here.

Irrespective of the exact failure mode, the molecular mechanism(s) responsible for the long-term failure of polymers is generally accelerated by stress and temperature. With the exception of polyethylene, which sometimes shows a change in failure kinetics at intermediate stresses,[8,9] the logarithm of the time-to-failure is observed to increase linearly with decreasing stress for the majority of polymers.[3] In some cases a lower stress limit is encountered below which no failure occurs, the so-called endurance limit.[4,10−12] The effect of temperature is straightforward, reducing the time-to-failure as temperature increases.[4,5,8,10,11] Decreasing the molecular weight has a similar effect, although it only appears to influence the brittle failure mode.[3,8,9] Orientation[11,13] and structural evolution, due to annealing,[14] slow cooling,[6,8,12,] and physical aging,[15] are known to increase the time-to-failure. While most materials show either brittle or ductile failure,[3] poly(vinyl chloride) and polyethylene are known to display ductile-to-brittle transitions at intermediate stress levels,[5,6,8,9] where the transition observed is accelerated by temperature.[4,5,8] The effect of the stress-state can point in different directions[16,17] and, while in laboratory tests the stress state is often uniaxial, in reality more complex stress states occur, showing different failure kinetics.[16−19]

The importance of preventing failure under long-term static loading is evident. It is also clear that the necessity to perform real-time experiments, over the entire lifetime of a polymer structure or component, is highly impractical. This is particularly the case when the influence of all the different parameters, mentioned above, has to be verified. Consequently there is a need for the development of methods and techniques to predict the long-term durability of polymer materials, preferably from short-term tests, and it is, therefore, not surprising that a considerable number of studies has been dedicated to this goal. These studies can roughly be divided into two categories. The first category is that of the molecular theories, which consider failure of either primary,[20,21] or secondary[22,23] molecular bonds as a stress-activated process. Although these theories have been applied successfully to the failure of many polymers, they have their limitations since they, for instance, cannot account for the previously mentioned occurrence of an endurance limit. The second category contains the approaches based on continuum mechanics theory. Most commonly they combine a proper constitutive equation, describing the polymer's (time-dependent) deformation with a suitable failure criterion, such as a critical level of strain,[14,15] a deviatoric (free) stored energy,[24−26] or a time-dependent yield stress.[26] In essence failure is regarded to occur instantaneously after initiation, which is the moment the failure criterion is met. In this second category we also find the fracture mechanics approaches that consider crack propagation to be the rate-determining step. Using a modified linear elastic fracture theory, it is possible to predict a time-to-failure under constant stress for both notched and homogeneous materials.[27,28]

* Corresponding author. E-mail: l.e.govaert@tue.nl.

10.1021/ma0504973 CCC: $30.25
Published on Web 07/08/2005

Although promising results have been obtained, there are reasons which prevent a more extensive use of these models. First, several models require the actual failure data to determine their model parameters and, as a consequence, they lack predictive capability. Second, the majority of the models is essentially one-dimensional, preventing them from being used in more realistic loading geometries. Finally, none of the models can account for the influence of thermal history (including processing). This implies that a change in processing history, or the application of a heat treatment, requires repeating the entire, often very laborious, characterization procedure. Consequently, all changes have to be validated in the actual product under operating conditions. The only remedy to these disadvantages is the development of a 3D constitutive equation (and failure criterion), which can account for differences in thermal history and molecular weight. This is the objective of the present research.

The failure modes generally observed in long-term failure involve a plastic instability, particularly in ductile failure. For glassy polymers under a constant rate of deformation, the formation of such plastic instabilities has been extensively studied, both experimentally[29] and numerically,[30−32] for short-term failure. Using three-dimensional constitutive models to describe the intrinsic deformation behavior, it was shown that the postyield behavior plays an essential role in the initiation and stabilization of strain localization in polymers.[30−32] To account for the influence of thermal history, a modification and extension of these models was presented and verified for different molecular weights.[33] This modification is based on the fully rejuvenated state that can be attained through application of a large plastic deformation erasing the initial state of the material. In time, the aged state is slowly recovered, a process that is accelerated by temperature and load applied.

In this article we show that long-term ductile failure is governed by the same process as short-term ductile failure and that the viscoelastic models developed for the second are therefore applicable for the first. To account for structural evolutions during the long-term loading we use the enhanced model presented in another publication.[33] First, the creep rupture response of the model is compared to experimentally obtained time-to-failure results on polycarbonate in different loading geometries. Second, the influence of thermal history is investigated experimentally for a high molecular weight polycarbonate, and compared to model predictions. Third, the influence of molecular weight is evaluated using a polycarbonate with a considerably lower molecular weight. Finally, all results are discussed and conclusions are drawn.

2. Experimental Section

2.1. Materials. Two different commercial grades of polycarbonate were used: Bayer Makrolon CD2000 and General Electric Lexan 121R. In addition we used an extrusion grade of Lexan (General Electric, type unknown) supplied as 6 mm diameter extruded rod, as well as an extrusion grade of Makrolon (Bayer, type unknown) supplied as 3 mm thick extruded sheet. Molecular weight distributions were determined using gel permeation chromatography (GPC), the resulting number-averaged and weight-averaged molecular weights are listed in Table 1.

Table 1. Weight-Averaged and Number-Averaged Molecular Weights of the Polycarbonate Grades Used in This Study Measured with Respect to a PC Standard

grade	M_n [kg/mol]	M_w [kg/mol]
Makrolon CD2000	8.2	18.7
Lexan 121R	9.8	23.4
Makrolon sheet	13.3	29.4
extruded rod	14.0	35.9

For uniaxial compression tests, cylindrical samples (o.d. 6 mm × 6 mm) were machined from either the extruded rod, or from plates (200 × 200 × 10 mm^3), that were compression molded from granular material at a temperature of 250 °C. First the dried granulate was heated for 15 min and next compressed up to 300 kN in five subsequent intervals of 5 min. After each step, the force was released to allow for degassing. Finally, the mold was placed in a cold press and cooled to room temperature (20 °C) under a moderate force (100 kN). Tensile samples were either prepared through injection molding or milled from compression molded plates (160 × 160 × 3 mm^3), molded according to the procedure outlined above. The geometry of all tensile specimens was according to ISO 527.

A separate set of samples for three different loading geometries was prepared from the Makrolon sheet. For uniaxial tensile tests, samples according to ASTM D638 and a thickness of 1.7 mm were milled from this sheet. For planar extension tests, rectangular samples with a dogbone-shaped cross-section were milled from the sheet, see Govaert et al.,[34] with in the testing region a thickness of 1.7 mm over a length of 10 mm and a width of 50 mm. Because of the large width-to-length ratio the contraction of the material is constrained, creating a plane strain condition.[35] For simple shear tests, samples similar to those used in the planar tests were used, now with a width of 100 mm instead of 50 mm. With a gauge length of 10 mm, this results in an aspect ratio of 10. To avoid any influence of orientation effects due to the extrusion process all samples were taken from the same direction.

2.2. Thermomechanical Treatments. Annealing of some of the samples was performed for 120 h in an air circulated oven at a temperature of 120 °C. Initial equilibration of the sample temperature was measured to take approximately 15 min. After a predefined aging time the samples were removed from the oven and allowed to cool to room temperature in air before being tested.

Mechanical preconditioning under dead-weight loading was performed either on a Zwick Rel servo-hydraulic tensile tester equipped with a temperature chamber or by using a long-term dead-weight setup at room temperature.

2.3. Mechanical Testing. Uniaxial compression tests were performed on a servo-hydraulic MTS Elastomer Testing System 810. The specimens were cylindrical shaped and compressed under true strain control, at constant true strain-rates of 10^{-4} to 10^{-2} s^{-1} between two parallel, flat steel plates. Friction between samples and plates was reduced by an empirically optimized method. Onto the sample ends was applied a thin film of PTFE tape (3M 5480, PTFE skived film tape), and the contact area between steel and tape was lubricated using a 1:1 mixture of liquid soap and water. During the test no bulging of the sample was observed, indicating that the friction was sufficiently reduced.

Uniaxial and planar tensile tests were performed on a Zwick Z010 tensile tester, at constant linear strain-rates of 10^{-5}−10^{-1} s^{-1}. Shear tests were performed on a Zwick 1475 at shear rates from 10^{-5}−10^{-2} s^{-1}. Stress−strain curves were recorded, and where appropriate, true stresses were calculated assuming a constant sample volume.

Constant load tests at high loads in uniaxial and planar extension were performed on a Zwick Z010 tensile tester, and in shear on a Zwick 1475. The load was applied in approximately 10 s, both force and displacement were monitored. Uniaxial constant load tests at comparatively medium and low stresses were performed under dead-weight load on a static load setup. At long loading times electronic timers were used to detect failure of a sample.

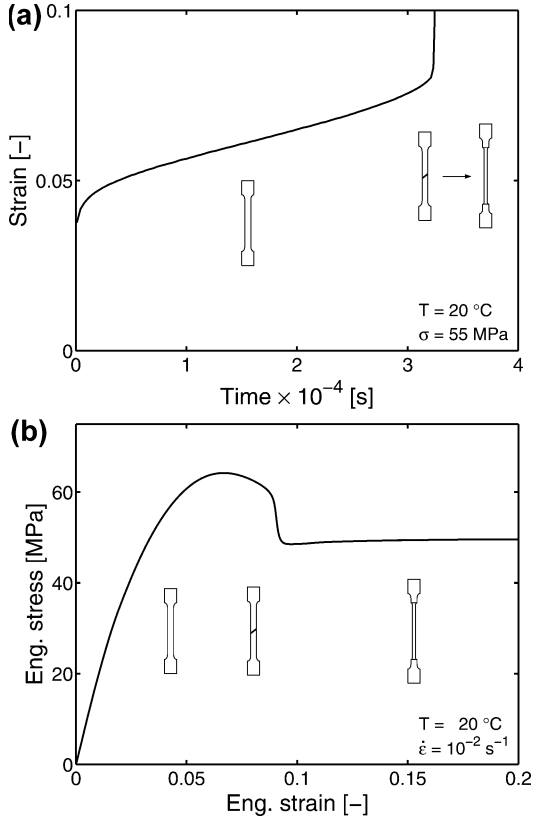

Figure 1. Deformation behavior of polycarbonate in uniaxial tension (a) under a constant load of 55 MPa and (b) at a constant strain-rate of 10^{-2} s^{-1}.

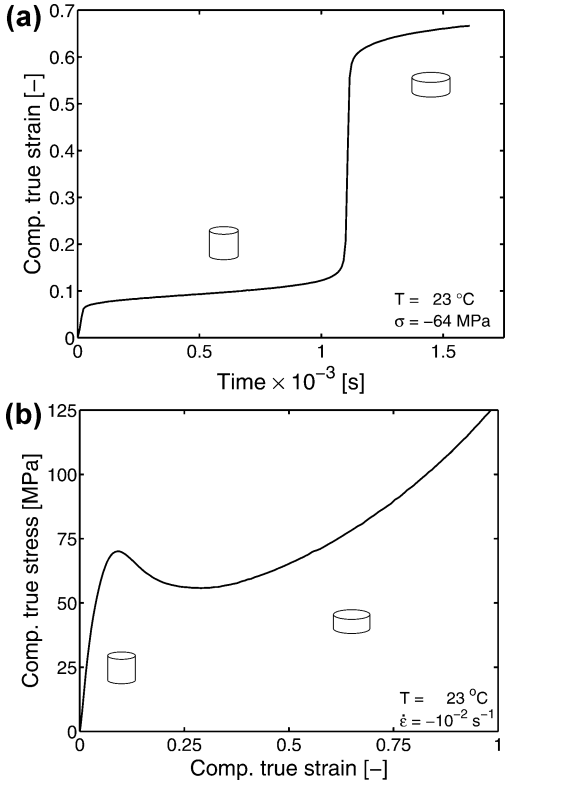

Figure 2. Intrinsic deformation behavior of polycarbonate in uniaxial compression (a) under a constant true compressive stress of 64 MPa and (b) at a constant true compressive strain rate of 10^{-2} s^{-1}.

3. Time-Dependent Ductile Failure: Relation to Intrinsic Behavior

An example of long-term time-dependent deformation is shown in Figure 1a. The evolution of creep strain for a polycarbonate sample subjected to a constant tensile load of 55 MPa is shown, as well as various marked stages of the macroscopic deformation. Initially, the sample deforms homogeneously at a decreasing rate until, after some time, a constant minimum creep rate is reached. After this stage, the creep rate increases again, finally resulting in the formation of a sudden neck that propagates rapidly along the length of the sample.

This typical pattern of homogeneous deformation, neck formation, and neck growth is also observed at a constant rate of deformation in a short term tensile test (Figure 1b). During the initial homogeneous deformation the stress rises until a maximum is reached, the yield stress. Shortly after the yield stress, a neck is formed that propagates at a constant rate and stress along the sample.

From numerical investigations it has become evident that the occurrence of plastic instabilities such as neck formation, but also crazing, is closely related to the intrinsic deformation behavior of polymer materials determined from constant true strain-rate compression experiments;[30–32] see Figure 2b. At relatively small deformations, the yield stress of the material is reached. With increasing strain the stress decreases, generally referred to as (true) strain softening. At even larger strains the stress rises again due to orientation of the polymer molecules: strain hardening. Both experimental and numerical studies showed that the post yield behavior plays an important role in strain localization phenomena. Initiation of the instability is triggered by strain softening, whereas strain hardening stabilizes the localization allowing it to grow.[29–32]

Now we can of course also compare this intrinsic behavior in a *constant true strain-rate* compression test (Figure 2b), with that in a *constant true-stress* compression experiment, Figure 2a. Upon loading, the strain increases at a decreasing rate, reaching a constant creep rate. After a long time of steady creep, the creep rate accelerates rapidly and the sample becomes compressed homogeneously in a relatively short time. At large strains this acceleration decreases strongly, and further creep proceeds at a strongly reduced rate. This behavior of Figure 2a includes the same features as described for the constant rate compression test in Figure 2b: yield, (true) strain softening, and strain hardening. This is illustrated more clearly by using a so-called Sherby–Dorn plot,[36] Figure 3, for different levels of applied stress.

The graphs show that, after applying the initial load, the creep rate decreases to a minimum level. It was shown by Bauwens-Crowet for polycarbonate,[37] and by Nanzai for poly(methyl methacrylate),[38] that this point is identical to the yield point observed in a constant strain-rate test. After passing the yield point, the material starts to soften which, due to the constant stress applied, results in a fast increase in creep rate and, therefore, creep strain. At sufficiently large strains, the orientation-induced strain hardening sets in, stabilizing the softening process and strongly reducing the creep rate (the vertical axis is logarithmic).

From these results, it is concluded that the intrinsic deformation under constant load already contains an inherent failure mechanism which is strain softening. While first deforming homogeneously, the onset of strain

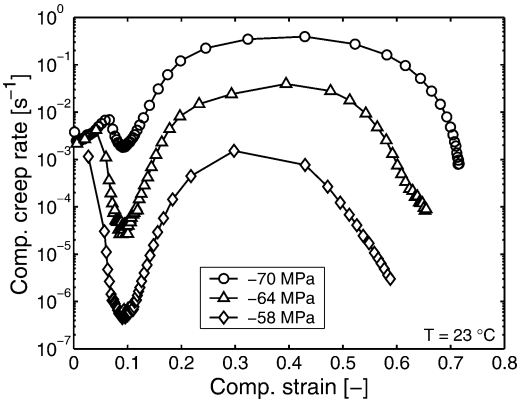

Figure 3. Sherby–Dorn plot for polycarbonate in uniaxial compression under three different compressive true stresses.

softening results in a sudden, large, increase of strain. Macroscopically, the strain softening phenomenon triggers a strain localization which manifests itself in the formation of a neck.

Because of the strong similarity between the intrinsic behavior under constant stress and that under constant strain rate, it is suggested that the 3D constitutive models used for the latter are applicable to constant load tests as well. In view of the larger time scales involved, such models should, however, also account for structural evolution due to physical aging. An example of such an approach was presented in a previous publication[33] and will be summarized below.

4. Constitutive Modeling

All 3D constitutive models for solid polymers start with the split of the total stress in two main contributions, based on the original work of Haward and Thackray[39]

$$\boldsymbol{\sigma} = \boldsymbol{\sigma}_s + \boldsymbol{\sigma}_r \tag{1}$$

where $\boldsymbol{\sigma}_r$ denotes the strain hardening contribution that is attributed to molecular orientation and is described by neo-Hookean behavior, and $\boldsymbol{\sigma}_s$ includes the contribution due to rate dependent plastic flow. This plastic flow process is represented by a nonlinear Maxwell model[40] as suggested by Baaijens.[41] Under isothermal conditions the nonlinearity of the model is completely governed by a stress, pressure, and state dependent viscosity η, which is defined as

$$\eta(T, \bar{\tau}, p, S) = \eta_{0,r}(T) \underbrace{\frac{\bar{\tau}/\tau_0}{\sinh(\bar{\tau}/\tau_0)}}_{\text{(I)}} \underbrace{\exp\left(\frac{\mu p}{\tau_0}\right)}_{\text{(II)}} \underbrace{\exp\left(S(t, \bar{\gamma}_p)\right)}_{\text{(III)}} \tag{2}$$

Here the part marked I, where $\bar{\tau}$ is the equivalent stress, represents the stress dependence of the viscosity governed by the parameter τ_0. Part II yields the pressure dependency governed by the parameter μ, and where p is the hydrostatic pressure. Part III represents the dependence of the viscosity on the state of the material expressed by the state parameter S. Finally $\eta_{0,r}(T)$ denotes the viscosity for the completely rejuvenated state.

The material state S is determined by two processes, physical aging, measured as an increase in yield stress, and mechanical rejuvenation during loading, measured as true strain softening. In the model, these two processes are decoupled: $S(t, \bar{\gamma}_p) = S_a(t)R_\gamma(\bar{\gamma}_p)$. In this expression the function R_γ describes the mechanical rejuvenation upon plastic deformation $\bar{\gamma}_p$ and is given by

Table 2. Material Parameters for Polycarbonate at a Reference Temperature of 23 °C

E [MPa]	ν	$\eta_{0,r}$ [MPa s]	τ_0 [MPa]	μ	S_a	r_0	r_1	r_2	G_r [MPa]
900	0.4	2.1×10^{11}	0.7	0.08	–	0.965	50	−5	26

c_0	c_1	t_a [s]	ΔU_a [kJ/mol/K]	$\bar{v}_a$ [m^3/mol]
−4.41	3.3	–	205	$1.33 \cdot 10^{-3}$

$$R_\gamma(\bar{\gamma}_p) = \frac{(1 + (r_0 \exp(\bar{\gamma}_p))^{r_1})^{(r_2-1)/r_1}}{(1 + r_0{}^{r_1})^{(r_2-1)/r_1}} \tag{3}$$

where $\bar{\gamma}_p$ denotes the equivalent plastic strain, and r_0, r_1, and r_2 are fitting parameters. The aging contribution is $S_a(t)$:

$$S_a(t_{eff}) = c_0 + c_1 \log\left(\frac{t_{eff}(t, T, \bar{\tau}) + t_a}{t_0}\right) \tag{4}$$

Here $t_0 = 1$ s, c_0 and c_1 are constants determined at a constant strain rate of 10^{-2} s^{-1}, t_a is the initial age, and t_{eff} is the effective time, defined as

$$t_{eff}(t, \bar{\tau}, T) = \int_0^t \frac{d\xi}{a_\sigma(\bar{\tau}(\xi))\, a_T(T(\xi))} \tag{5}$$

where a_σ is a stress activation of the Eyring type and a_T is a temperature shift function of the Arrhenius type.

In previous work the details of the model and all relevant material parameters were given, partly reproduced in Table 2. Values for the parameter S_a, the initial value for S at the initial age t_a, are not provided since they are determined for each material separately measuring the yield stress at a single strain-rate.

To demonstrate the model's capability, constant strain-rate compression tests were numerically simulated and compared to experimental results; see Figure 4a, which shows an excellent description of the strain rate dependence of both the yield and postyield behavior. Because of the single mode representation, the preyield behavior is not captured accurately. Employing a multimode representation will improve on this significantly.

Figure 4b shows that also for different initial ages the yield and postyield behavior is captured well by the model. At large strains the calculated stresses coincide, something which has also been observed in experiments on various polymers.[29,42,43]

5. Application to Time-Dependent Ductile Failure

5.1. Influence of Loading Geometry. The loading geometry is known to play an important role in deformation and failure. This is shown by the true yield stresses obtained for polycarbonate strained at different rates in three different loading geometries, Figure 5a. The response is strongly geometry dependent in both the magnitude of the yield stress as well as its rate dependence. Identical trends can be observed in the time-to-failure of creep rupture experiments where a constant load is applied to the same material until either a neck or shear band is formed, Figure 5b.

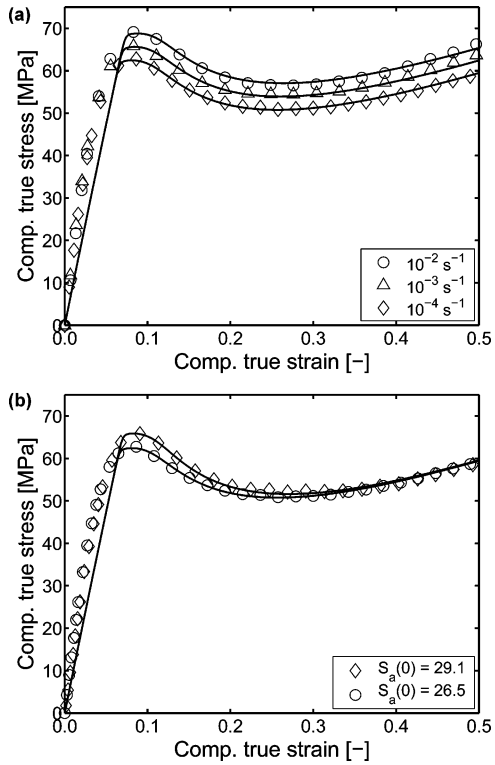

Figure 4. Comparison of model predictions (solid lines) to experimental results (symbols) for (a) different strain rates and (b) quenched (○) and annealed (◇) samples.

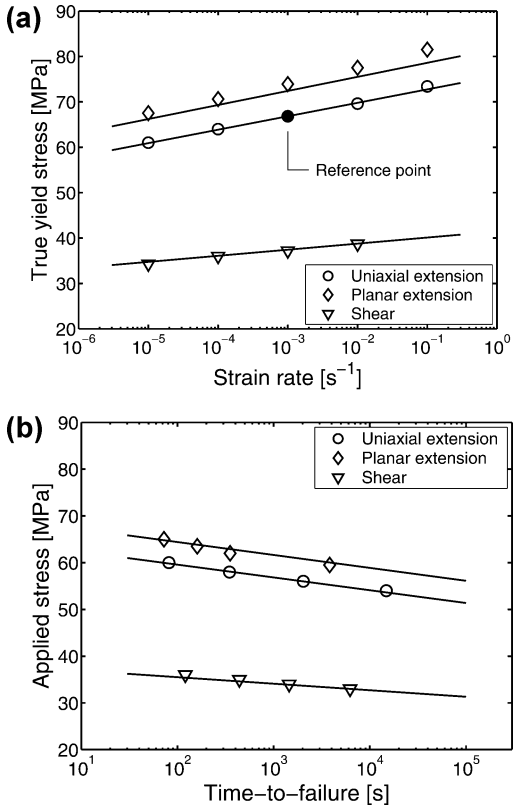

Figure 5. (a) True yield stress vs strain rate for polycarbonate in three different loading geometries and (b) applied stress vs time-to-failure for polycarbonate in three different loading geometries. Symbols indicate experimental results, and solid lines represent model predictions.

Finite element simulations were performed using full three-dimensional meshes of the uniaxial, planar, and shear samples used in the experiments, consisting of 2130, 3760, and 7520 eight-node linear brick elements, respectively. During the constant rate of deformation tests, the samples were deformed at constant linear strain rates from 10^{-5} to 10^{-1} s^{-1}, similar to the actual experiments. Time-to-failure for different constant loads was predicted by applying a load to the samples in 10 s, conforming to the average experimental application time, and sustaining this load accordingly. For the constant load calculation, the time step is controlled by an adaptive time stepping scheme based on a critical strain increment. The actual failure time is defined as the time at which a strain localization, which can be either a neck or a shear band, is formed and starts propagating.

To enable numerical simulations, the initial value of the state parameter S was fitted using the experimental yield stress in uniaxial extension at a single strain rate of 10^{-3} s^{-1} as the reference point (see the single filled symbol in Figure 5a). This resulted in a value for $S_a(0)$ of 31.1, or, using eq 4, an initial age t_a of 5.76×10^{10} seconds. Using the general parameter set of Table 2 and the fitted values for S_a or t_a, an excellent description of both the magnitude and rate dependence of the true yield stresses is found for each loading geometry: compare the solid lines (model predictions) and the symbols (experiments) in Figure 5a. In the numerical calculations of the constant load experiments of Figure 5b, aging did not have to be taken into account; i.e., t_{eff} in eq 4 is set to zero, given the relatively short experimental time scale. The results of the model predictions (solid lines) of the constant load experiments (symbols) are shown in Figure 5b. From this figure, it is clear that the model accurately predicts both the stress dependence as well as the magnitude of the times-to-failure for the three different loading geometries used in this investigation.

5.2. Influence of Thermal History. Thermal history has a profound influence on the initial state of a polymeric material and, thus, on its (macroscopic) deformation and failure. Therefore, two different sets of samples were prepared, one via annealing. Tensile tests on these two sets revealed a significant increase in yield stress for the annealed specimens, whereas the strain rate dependence remained unaffected (Figure 6a), which corresponds to similar observations by Bauwens-Crowet and Bauwens.[44]

Subsequently, creep rupture experiments were performed where samples are subjected to a constant load until either a neck is formed, or the sample breaks. Both sets of samples formed a neck, although the annealed samples fractured shortly after necking. The experimental results show a strong resemblance to the tensile results in that, for a given time, the annealed samples can sustain a higher load than the quenched samples, and that the stress dependence is independent of the thermal history (Figure 6b). Similar to the experiments of Narisawa et al.,[12] the quenched materials show what appears to be the onset of an endurance limit.

Finite element simulations were performed using an axisymmetric model of a tensile bar with a small imperfection in the middle. This cylindrical tensile bar has a parallel length of 1 and a radius of 0.2. The circular imperfection has a radius of 0.02 and a maximum depth of 0.003, which is 1.5% of the bar's radius.[29] The finite element mesh consists of 537 8-node second-order elements.[29] Furthermore, the same procedure as

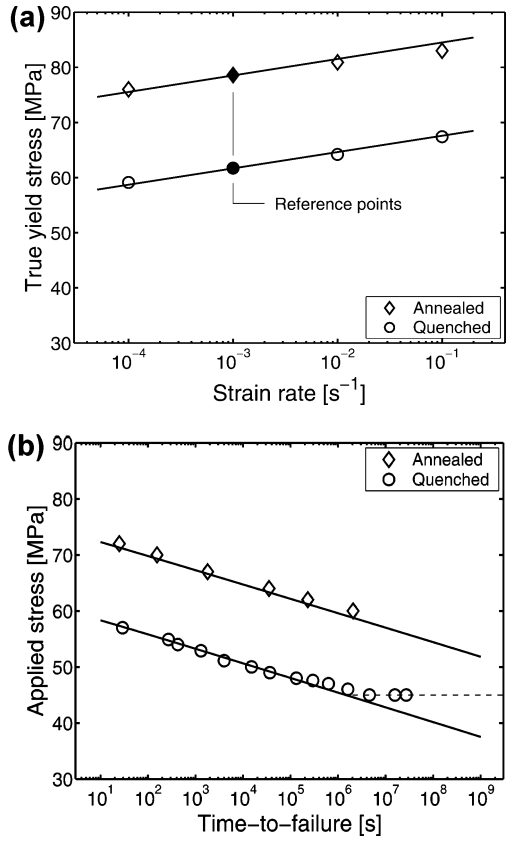

Figure 6. (a) True yield stress vs strain rate for quenched and annealed polycarbonate and (b) applied stress vs time-to-failure for quenched and annealed polycarbonate. Symbols indicate experimental results, and solid lines represent model predictions (aging not taken into account).

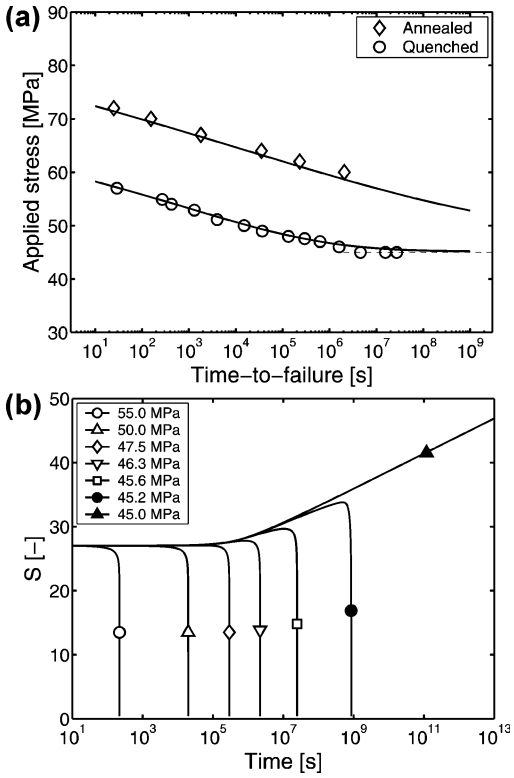

Figure 7. (a) Comparison of experimental results (symbols) with numerically predicted failure times using the model including aging (solid lines) for both quenched and annealed material. (b) Evolution of the state parameter S as a function of time for the quenched material at different stress levels.

in the previous section was applied for the prediction of tensile and creep rupture tests.

The resulting fitted values for $S_a(0)$ were 27.5 and 40.7, and the initial ages t_a were 4.67×10^9 and 4.67×10^{13} seconds for the quenched and the annealed material, respectively. Using the general parameter set of Table 2, and the fitted values for S_a or t_a, an excellent description of magnitude and strain rate dependence of the yield stress is found, see Figure 6a. When, to a first approximation, aging is not taken into account in the constant load experiments, i.e., in eq 4 t_{eff} is again set to zero, the results for the long-term prediction shown in Figure 6b are obtained. Despite the limited range of strain rates used to characterize the kinetics, it is clear from this figure that the stress dependence of the failure times is predicted very well over a large range of stresses and times. The reasons for this successful extrapolation was demonstrated by Bauwens-Crowet et al.,[37] who showed that for polycarbonate the yield behavior in both tensile and creep loading is governed by a single process. In addition to the prediction of the stress dependence of the times-to-failure, Figure 6b also shows that the difference in initial state is extremely well accounted for. In contrast to the experimental results, the model predicts, however, no endurance limit for the quenched material.

This changes, however, drastically when aging is taken into account by including eqs 4 and 5 in the calculation, and relating, as a first approximation, the stress-activated part of the effective time expression (eq 5) to the applied stress rather than the local stress. From Figure 7a, it can be seen that the incorporation of aging leads to a considerable improvement of the prediction for the quenched material including an endurance limit at 45 MPa.

The origin of this improvement in prediction, and the existence of an endurance limit, is clarified in Figure 7b, displaying the local evolution of the state parameter S with time for the quenched material at different applied loads in a representative node on the axis of symmetry below the imperfection. At high stresses and short failure times, the material rejuvenates (S goes to zero) since strain softening decreases the parameter S. With decreasing loads, and thus increasing loading times, the influence of the stress accelerated aging process becomes noticeable. For small loads and long times this process becomes dominant resulting in an increase in S, and consequently an increase in the yield stress and a reduction in creep rate and thus the prevention of an accumulation of plastic strain. As a result, softening can no longer occur, and the material no longer fails by necking.

5.3. Influence of Molecular Weight: A Tough-to-Brittle Transition. Until now we only used a single polycarbonate grade (Lexan 121R) of relatively high molecular weight. In the Introduction it was, however, already pointed out that failure is affected by molecular weight. A decrease in molecular weight can lead to a reduction of failure times sometimes accompanied by a change in failure mode.[3,8,9]

In a previous publication,[33] it was shown that, provided that the thermal history is the same, the intrinsic deformation behavior of polycarbonate is independent of the molecular weight. This is confirmed once more in Figure 8 which shows the strain rate dependence of the yield stress for a high (Lexan 121R), and low

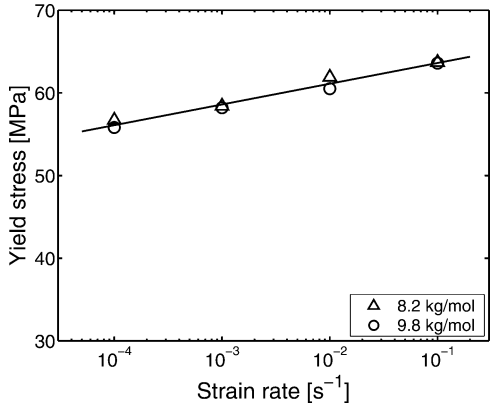

Figure 8. Comparison of the strain rate dependence of the yield stress for a low (CD2000), and high molecular weight polycarbonate (121R). Symbols indicate experimental results, and the solid line is a linear fit to guide the eye.

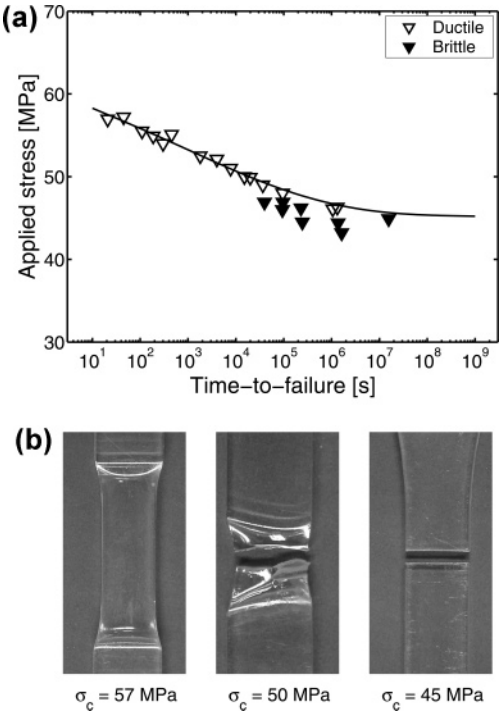

Figure 9. (a) Applied stress vs time-to-failure for the low molecular weight polycarbonate (CD2000), symbols indicate experimental results and the solid line is the model prediction from Figure 7a. (b) Macroscopic failure behavior of low molecular weight polycarbonate at different loads applied.

molecular weight (Makrolon CD2000) polycarbonate having identical thermal histories.

On the basis of this observation and the results of the previous sections, it can be anticipated that creep rupture of the low molecular weight material is identical to that of the high molecular weight material and that, consequently, the numerical results obtained for the high molecular weight material also apply to the low molecular weight material.

Actual creep rupture experiments performed on the low molecular weight material show that this is only partially true, Figure 9a. For high stresses, the failure kinetics are indeed the same and, here, both grades fail ductile through neck-formation. With decreasing stress, the time to failure increases and the failure mode for the low molecular weight material gradually changes to brittle. In the transition zone, a neck is still formed, but fails shortly after initiation; see Figure 9b. At this stage, locally fairly large strains can still be observed. With further decrease of the stress applied, the plastically deformed zone becomes smaller until finally the failure becomes completely brittle; see the filled symbols in Figure 9a.

Despite the change in failure mode, Figure 9a clearly shows that the failure kinetics are not significantly influenced. This is in line with observations reported in the literature for poly(vinyl chloride)[5] and polyethylene.[4,6] The change in failure kinetics observed for polyethylene at elevated temperatures[8,9] was attributed to oxidative thermal degradation, reducing the molecular weight *during* the experiment, by Gedde et al.[45] Results by Crissman and McKenna[14] on poly(methyl methacrylate) indicate that a decrease in molecular weight (caused by long-term annealing *before* the creep test) reduces the time-to-failure, but does not influence the failure kinetics. This is consistent with the creep rupture behavior observed by Gotham[3] for a low and high molecular weight poly(methyl methacrylate). While the high molecular weight material failed ductile, the lower molecular weight material failed brittle. The failure kinetics of both materials were, however, identical. Combined with our results this suggests that, rather than two separate mechanisms, a single mechanism is responsible for both ductile and brittle failure in long-term loading.

The existence of a ductile-to-brittle transition is often explained by means of a critical strength above which the material fractures rather than showing ductile failure. If this approach is applied to creep rupture experiments it would predict a transition with *increasing* load, i.e., as the applied stress on the material is increased. In literature such a transition at high loads is known, and reported for several materials.[1] However, using such a critical strength criterion for *decreasing* loads will not result in a transition, since a decreasing load implies decreasing stress levels, and a polymer material that fails ductile at a given stress will therefore fail ductile at any other lower stress.

An alternative explanation is provided by the combination of time and stress applied, rather than the stress level alone. It has been shown experimentally that applying a constant load for a given amount of time accelerates the aging process, increasing the yield stress.[33,46–51] From the numerical results in the previous section we concluded that aging during testing induces a change in the macroscopic behavior leading to an endurance limit. Associated with this endurance limit is an increase in the parameter S, which is equivalent to an increase in the yield stress.

To verify whether this change in the material leads to embrittlement in the case of a low molecular weight polycarbonate, an initially ductile sample (Figure 10a, left) is subjected to a constant load of 45 MPa for 2 days. After this treatment the material failed brittle under the same testing conditions (middle). Bringing a sample with an identical history above the glass transition temperature for half an hour, followed by a quench to room temperature, restored the original ductile behavior (right), indicating that the change observed in failure mode is thermoreversible and therefore not caused by degradation.

A similar change in the macroscopic failure behavior of polycarbonate was reported by van Melick et al.,[29] who observed a ductile-brittle transition as a result of

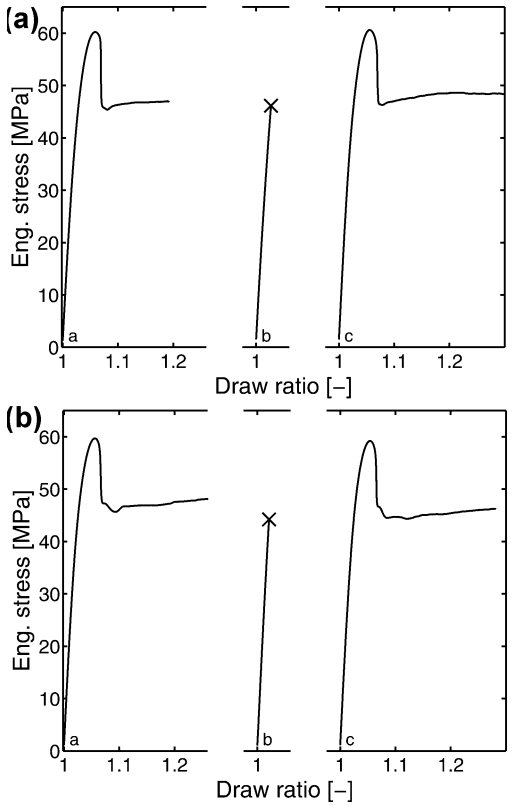

Figure 10. (a) Influence of mechanical history (constant load) on the macroscopic deformation behavior of low molecular weight polycarbonate. (b) Influence of thermal history (annealing) on the macroscopic failure behavior of low molecular weight polycarbonate.[29]

thermal history, annealing an initially ductile low molecular weight polycarbonate (Figure 10b, left) for 120 h at 120 °C. After this thermal treatment the material failed brittle (middle), whereas heating an annealed sample again, now above the glass transition temperature for half an hour, and cooling rapidly to room temperature, restored the original ductile behavior (right), indicating that the change observed in failure is again thermoreversible and not caused by degradation due to long-term annealing.

Van Melick et al. rationalized this change in macroscopic behavior by comparing the intrinsic deformation behavior of a quenched and annealed polycarbonate.[29] The thermal treatment causes an increase in yield stress and, consequently, an increase in the amount of strain softening upon mechanical rejuvenation during deformation. Strain hardening is, on the other hand, unaffected. The higher yield stress and enhanced strain softening require a higher draw ratio for the neck to stabilize, thus increasing the true stress in the necked region. When this stress exceeds the strength of the material, which is determined by the molecular weight, premature fracture rather than stable neck propagation occurs.[29]

The approach by van Melick et al. provides a criterion which is essentially a molecular weight dependent critical strength above which a neck cannot sustain the load it is subjected to. As stated previously, for creep tests such a criterion only predicts a transition for increasing stress levels. Despite the change in material properties with decreasing load and increasing time it follows from the analysis by van Melick et al. that still no transition will occur with decreasing load. This can be understood since for the latter the stress in the neck is dictated by the (decreasing) load applied, while for a constant rate of deformation test it is determined by the changing, state-dependent, yield stress. The prediction of a ductile-to-brittle transition with decreasing loads, therefore, requires a different approach.

The basic assumption of the analysis by van Melick et al. is that there already is a neck, and they only verify if this neck can exist (ductile), or not (brittle). The formation of a neck, however, involves the evolution of localized deformation zones, triggered by inhomogeneities in the local stress field, and is influenced by the amount of strain softening. The resulting concentration of deformation leads to changes in the local stress distribution enhancing any deviation from the macroscopical stress applied. If during this localization process some local failure criterion is exceeded this results in brittle failure, and no neck will be formed (and hence the analysis of van Melick et al. is not applicable). An example of such a local criterion is the critical hydrostatic stress which has been shown to be effective in predicting local craze initiation.[52] The fact that this failure process is preceded by local plastic deformation would also explain the observed similarity between the failure kinetics of the ductile and brittle failure mode.

The identification of the actual local failure criterion requires knowledge of the local state of the material and stress. Unfortunately, these are generally unknown. This can be solved by investigating the local stress state in well-defined stress concentrations (e.g., notches, microstructure, indentation) using numerical techniques,[53,54] but preferably in combination with an experimental verification.[52,55] This requires further research and is outside the scope of this work.

6. Conclusions

The long-term failure behavior of polycarbonate under constant static load was investigated. It is shown that ductile failure observed under these conditions is similar to that observed in short term tests under constant rate of deformation.

To model long-term failure, an elastoviscoplastic model, incorporating aging kinetics, was employed. The model was shown to accurately predict both magnitude and stress dependence of the time-to-failure of polycarbonate in three different loading geometries, using a single yield stress to determine the initial age. With similar accuracy the time-to-failure for two sets of materials with different thermal histories was predicted, again using a single yield stress to determine the initial age of each set. Furthermore, the endurance limit, observed for the quenched material, could be predicted quantitatively when the material was allowed to also age during the numerical calculation.

Reducing the molecular weight does not introduce changes in the short-term failure behavior, neither under constant rate of deformation, nor under constant load. For reducing loads and increasing failure times, however, the structural evolution causes an increased localization due to which locally the strength of the material is exceeded. Although it is clear from the experiments that a suitable failure criterion enabling a quantitative prediction of brittle failure depends on molecular weight, the identification of an actual criterion requires further research.

Acknowledgment. The authors wish to acknowledge Bas Raas for his contribution to the experimental

work performed in the group of Warner Nauta at TNO Industrial Technology.

References and Notes

(1) Kausch, H. H. *Polymer Fracture*; Springer-Verlag: Berlin, 1978.
(2) Kinloch, A. J.; Young, R. J. *Fracture Behaviour of Polymers*; Elsevier Applied Science Publishers: London, 1985.
(3) Gotham, K. V. *Plast. Polym.* **1972**, *40*, 59−64.
(4) Crissman, J. M.; Zapas, L. J. *Polym. Eng. Sci.* **1979**, *19*, 99−103.
(5) Niklas, H.; Kausch von Schmeling, H. H. *Kunststoffe* **1963**, *53*, 886−891.
(6) Teoh, S. H.; Cherry, B. W. *Polymer* **1984**, *25*, 727−734.
(7) Lustiger, A. Environmental stress cracking: the phenomenon and its utility. In *Failure of Plastics*; Booth, C., Price, C., Eds.; Hanser Publisher: New York, 1986.
(8) Cooney, J. L. *J. Appl. Polym. Sci.* **1964**, *3*, 1889−1901.
(9) Richard, K.; Gaube, E.; Diedrich, G. *Kunststoffe* **1959**, *49*, 516−525.
(10) Matz, D. J.; Guldemond, W. G.; Cooper, S. L. *J. Polym. Sci.: Polym. Phys. Ed.* **1972**, *10*, 1917−1930.
(11) Ender, D. H.; Andrews, R. D. *J. Appl. Phys.* **1965**, *36*, 3057−3062.
(12) Narisawa, I.; Ishikawa, M.; Ogawa, H. *J. Polym. Sci.: Polym. Phys. Ed.* **1978**, *16*, 1459−1470.
(13) Richard, K.; Diedrich, G.; Gaube, E. *Kunststoffe* **1960**, *50*, 371−375.
(14) Crissman, J. M.; McKenna, G. B. *J. Polym. Sci., Part B: Polym. Phys.* **1990**, *28*, 1463−1473.
(15) Crissman, J. M.; McKenna, G. B. *J. Polym. Sci., Part B: Polym. Phys.* **1987**, *25*, 1667−1677.
(16) Crawford, R. J.; Benham, P. P. *Plast. Polym.* **1975**, *8*, 140−142.
(17) Gisolf, J. H.; van Goudoever, H. *Kunststoffe* **1959**, *49*, 264−268.
(18) Ogorkiewicz, R. M.; Sayigh, A. A. M. *Br. Plast.* **1967**, *7*, 126−128.
(19) Gaube, E. *Kunststoffe* **1959**, *49*, 446−454.
(20) Zhurkov, S. N. *Int. J. Frac. Mech.* **1965**, *1*, 311−323.
(21) Bueche, F. *J. Appl. Phys.* **1957**, *28*, 784−787.
(22) Tobolosky, A.; Eyring, H. *J. Chem. Phys.* **1943**, *11*, 125−134.
(23) Coleman, B. D. *J. Polym. Sci.* **1956**, *20*, 447−455.
(24) Teoh, S. H.; Cherry, B. W.; Kausch, H. H. *Int. J. Damage Mech.* **1992**, *1*, 245−256.
(25) Raghavan, J.; Meshii, M. *Mater. Sci. Eng.* **1995**, *A197*, 237−249.
(26) Brinson, H. F. *Comput. Struct.* **1999**, *47*, 445−456.
(27) Beaumont, P. W. R.; Young, R. J. *J. Mater. Sci.* **1975**, *10*, 1334−1342.
(28) Young, R. J.; Beaumont, P. W. R. *Polymer* **1976**, *17*, 717−722.
(29) Van Melick, H. G. H.; Govaert, L. E.; Meijer, H. E. H. *Polymer* **2003**, *44*, 3579−3591.
(30) Wu, P. D.; van der Giessen, E. *Int. J. Sol. Struct.* **1993**, *31*, 1493−1517.
(31) Wu, P. D.; van der Giessen, E. *Int. J. Plast.* **1993**, *11*, 211−235.
(32) Govaert, L. E.; Timmermans, P. H. M.; Brekelmans, W. A. M. *J. Eng. Mater. Techn.* **2000**, *122*, 177−185.
(33) Klompen, E. T. J.; Engels, T. A. P.; Govaert, L. E.; Meijer, H. E. H. *Macromolecules* **2005**, *38*, 6997.
(34) Govaert, L. E.; Schellens, H. J.; Thomassen, H. J. M.; Smit, R. J. M.; Terzoli, L.; Peijs, T. *Composites: Part A* **2001**, *32*, 1697−1711.
(35) Whitney, W.; Andrews, R. D. *J. Polym. Sci., Polym. Symp.* **1967**, *16*, 2981−2990.
(36) Sherby, O. D.; Dorn, J. E. *J. Mech. Phys. Solids* **1958**, *6*, 145−162.
(37) Bauwens-Crowet, C.; Ots, J.-M.; Bauwens, J.-C. *J. Mater. Sci. Lett.* **1974**, *9*, 1197−1201.
(38) Nanzai, Y. *JSME Int. J. Ser. A* **1994**, *37*, 149−154.
(39) Haward, R.; Thackray, G. *Proc. R. Soc. London A* **1968**, *302*, 453−472.
(40) Tervoort, T. A.; Smit, R. J. M.; Brekelmans, W. A. M.; Govaert, L. E. *Mech. Time-Dep. Mater.* **1998**, *1*, 269−291.
(41) Baaijens, F. P. T. *Rheol. Acta* **1991**, *30*, 284−299.
(42) Hasan, O. A.; Boyce, M. C.; Li, X. S.; Berko, S. *J. Polym. Sci., Part B: Polym. Phys.* **1993**, *31*, 185−197.
(43) Adam, G. A.; Cross, A.; Haward, R. N. *J. Mater. Sci.* **1975**, *10*, 1582−1590.
(44) Bauwens-Crowet, C.; Bauwens, J.-C. *Polymer* **1982**, *23*, 1599−1604.
(45) Gedde, U. W.; Viebke, J.; Leijström, H.; Ifwarson, M. *Polym. Eng. Sci.* **1994**, *34*, 1773−1787.
(46) Vincent, P. I. *Polymer* **1960**, *1*, 7−19.
(47) Kramer, E. J. *J. Appl. Phys.* **1970**, *41*, 4327−4341.
(48) Struik, L. C. E. *Polymer* **1980**, *21*, 962−967.
(49) Nanzai, Y.; Miwa, A.; Cui, S. Z. *Polym. J.* **2000**, *32*, 51−56.
(50) Nanzai, Y.; Cui, S. Z. *J. Polym. Sci., Part B: Polym. Phys.* **2001**, *33*, 444−449.
(51) Cui, S. Z.; Nanzai, Y.; Yoshioka, S. *Kobunshi Ronbunshu* **2000**, *57*, 37−44.
(52) Van Melick, H. G. H.; Bressers, O. F. J. T.; den Toonder, J. M. J.; Govaert, L. E.; Meijer, H. E. H. *Polymer* **2003**, *44*, 2481−2491.
(53) Smit, R. J. M.; Brekelmans, W. A. M.; Meijer, *J. Mater. Sci.* **2000**, *35*, 2855−2867.
(54) Smit, R. J. M.; Brekelmans, W. A. M.; Meijer, H. E. H. *J. Mater. Sci.* **2000**, *35*, 2869−2879.
(55) Van Melick, H. G. H.; Govaert, L. E.; Meijer, H. E. H. *Polymer* **2003**, *44*, 457−465.

MA0504973